

Jan Tomaszewicz*, Piotr Czarnocki

Warsaw University of Technology, Institute of Aeronautics and Applied Mechanics, ul. Nowowiejska 24, 00-665 Warsaw, Poland

**Corresponding author. E-mail: jan.tomaszewicz@meil.pw.edu.pl*

Received (Otrzymano) 27.02.2016

WING-TO-FUSELAGE ATTACHMENT FITTING FOR COMPOSITE AIRFRAMES - EXPERIMENTAL AND FINITE ELEMENT ANALYSIS

The design of a wing-to-fuselage attachment fitting for composite airframes is a considerable problem since it involves the application of point load to a laminate displaying a relatively low bearing strength. Nowadays the majority of composite airframes are made with the use of CF preimpregnates which make the solution to this problem even more involving. Recently, a new manufacturing technique has been developed that allows for the fabrication of a non-adhesive metal-composite joint especially designed to be used as wing-to-fuselage attachment fittings in the case of composite airframes made with VBO prepregs. In the body of the paper, first, a concise description of the manufacturing process of such a joint was provided, next, numerical stress analysis of the joint supplemented with experimental results was given. The experimental work concerned strain distribution and damage assessment investigated with the help of DIC and CT, respectively.

Keywords: metal-composite joints, prepregs, attachment point, finite element analysis, NAMCJ

BADANIA DOŚWIADCZALNE I ANALIZA MES MECHANIZMU PRZENOSZENIA OBCIĄŻENIA PRZEZ BEZADHEZYJNE POŁĄCZENIE METAL/KOMPOZYT

Połączenie skrzydło-kadłub w przypadku struktur kompozytowych stanowi poważny problem konstrukcyjny. Wynika to z konieczności wprowadzenia obciążeń skupionych w struktury kompozytowe charakteryzujące się niewielką odpornością na naciski. Współczesne lotnicze konstrukcje kompozytowe często wykonywane są z preimpregnatów węglowych, co jeszcze bardziej utrudnia rozwiązanie zadania. Ostatnio została opracowana nowa metoda wytwarzania bezadhezyjnych połączeń metal-kompozyt specjalnie zaprojektowanych w odniesieniu do takich celów i laminatów wykonanych z z preimpregnatów utwardzanych poza autoklawem z wykorzystaniem jedynie worka próżniowego. W artykule przedstawiono w skrócie technikę wytwarzania takiego połączenia oraz wyniki numerycznej analizy sposobu przenoszenia obciążeń przez takie połączenia wraz z doświadczalną weryfikacją obliczeń numerycznych, dokonaną za pomocą DIC. Wyniki uzupełniono obrazami pojawiających się w strukturze kompozytowej zniszczeń, narastających wraz ze wzrostem obciążenia. Wykazano, że w przypadku takiego połączenia w przenoszeniu obciążenia z elementów metalowych na kompozyt bierze udział kompozyt znajdujący się zarówno przed, jak i za elementami metalowymi, odmiennie jak ma to miejsce w przypadku zastosowania tradycyjnego połączenia sworzniowego, dla którego obciążenie przenoszone by było jedynie przez kompozyt znajdujący się przed sworzniem. Ponadto zidentyfikowano główne postacie zniszczenia oraz ich sekwencję. Były to: zerwanie włókien wzmocnienia, pęknięcia w spoiwie i zapoczątkowane nimi delaminacje oraz ścięcie laminatu powodowane ścisaniem. Jako pierwsze wystąpiło ścięcie laminatu na skutek ściskania, a następnie delaminacje oraz zerwanie włókien.

Słowa kluczowe: połączenia metal-kompozyt, prepregi, okucia, analiza MES, BPMK

INTRODUCTION

In the case of conventional metal structures, point loads can be applied with the help of bolts. Metals can yield and a perfect fit of the contacting bolt and hole surfaces can be reached after loading. Furthermore, metals display relatively good bearing strength. All of this is not the case of CF/epoxy laminates since they display negligible plastic deformation and do not yield, and are of relatively low bearing strength. Such mechanical properties of CR/epoxy laminates make the introduction of point loads difficult. So far, a few solutions

to this problem have been found (Fig. 1). They consist in taking advantage of metal adapters. Adapters can be in the form of metal bushes glued into the laminate structure (Fig. 1a). In this case, due to glue a perfect fit between the bush and laminate is reached that helps in more uniform distribution of the bearing stresses over the hole surface. Moreover, point loads can be applied via metal tiles (Fig. 1b), glued to the external laminate surfaces or metal inserts glued between the laminate layers (Figs. 1c and d) [1-3].

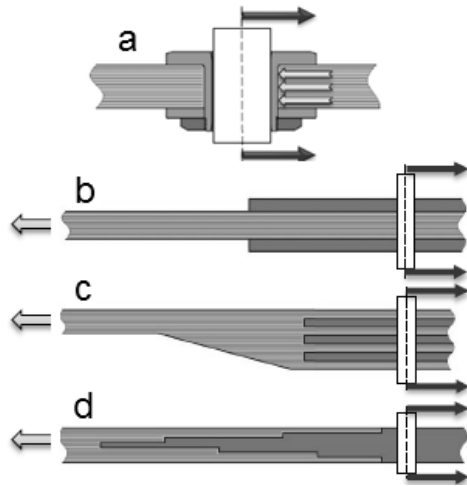


Fig. 1. Conventional ways of applying point loads to laminate shells or plates

Rys. 1. Tradycyjne sposoby wprowadzania obciążeń skupionych w płyty i powłoki kompozytowe

In all the mentioned designs, the gluing process can be complicated since chemical surface preparation of the composite and metal parts is crucial and the adhesive curing requirements must be strictly observed [4]. In addition, care must be taken to properly select metals to avoid galvanic corrosion. The non-adhesive metal-composite joint (NAMCJ) presented in this paper was used for wing-to-fuselage main attachments in several glider and motor glider designs completed at WUT. The joint is schematically shown in Figure 2. Such joints are non-adhesive since no adhesive is used to make them and in this way a majority of the aforementioned problems is eliminated. Previous investigations [5] related to the mechanical properties of the NAMCJ concerned its application in composite structures made with the use of the wet lay-up technique.

Several versions of the NAMCJ were designed. The presented one was especially designed for application in CF/epoxy structures made of Vacuum Bag Only (VBO) prepregs. In the joint of interest, the laminate plate or shell (1) is clamped between metal bushes (2), which in turn are tightened with a tapped sleeve (3) and nut (4). Due to such a design, the laminate is loaded in front of and behind the bolt (5) which is not the case of the design shown in Figure 1a, in addition, preparation of the adherent surfaces is eliminated unlike for the designs in Figures 1b-d.

This paper is focused on the strength and failure analysis of NAMCJ. At first, a concise description of the manufacturing process of such a joint is provided, then numerical stress analysis of the joint is presented. It is complemented with the corresponding experimental results. The experiments concerned strain distribution and damage assessment. Testing was carried out with the help of DIC and CT, respectively. The test specimen used for the investigation represented a joint introducing point load into the bulkhead. Such a joints are essential parts of the wing-to-fuselage attachment fitting (Fig. 2).

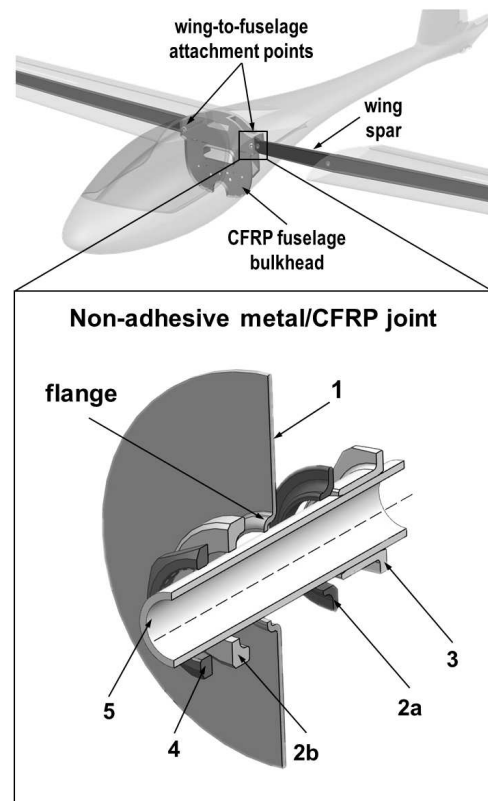


Fig. 2. Innovative non adhesive composite-metal joint used for wing-to-fuselage attachment fitting of motor glider AOS-71

Rys. 2. Innowacyjne bezadhezyjne połączenie kompozyt-metal wykorzystane w okuciach głównych połączenia skrzydła-kadłub motocybowca AOS-71

SPECIMEN. STRUCTURE AND MANUFACTURING

The metal parts of the joint were made with X17CrNi16-2 stainless steel by milling (Fig. 3). The composite structure consisted of 11 layers of MTM46/CF0300 VBO prepreg. It was reinforced with 2x2 twill fabric of areal weight 199 g/m² and contained 40% resin, by weight. The lay-up sequence was the following (Reinforcement orientations are given relative to the loading direction):

$[(\pm 45^\circ)/(0^\circ, 90^\circ)/(\pm 45^\circ)/(0^\circ, 90^\circ)/(\pm 45^\circ)/(0^\circ, 90^\circ)/(\pm 45^\circ)/(0^\circ, 90^\circ)/(\pm 45^\circ)/(0^\circ, 90^\circ)/(\pm 45^\circ)]$.

The manufacturing process of the joint was as follows (Fig. 4): First, the lower bush (2a) and the lower part of the external grip were nested in the mold and an appropriate number of prepreg layers of the prescribed reinforcement orientation sequence were laid down on the bush (2a) surface to form a flange. Next the upper bush (2b) was pushed into place and both the bushes were tightened with sleeve (3) and nut (4). Finally, the upper part of the external grip was put on the top of the prepreg pile and both the grip parts were clamped with screws. Such a set was put into a vacuum bag and cured for 8 h at 80°C and 0.1 MPa vacuum pressure then it was disassembled and the composite part (test piece) was free-standing post-cured at 135°C for 1.5 h. After post-curing, nut (4) was tightened with a tightening torque of 75 Nm.

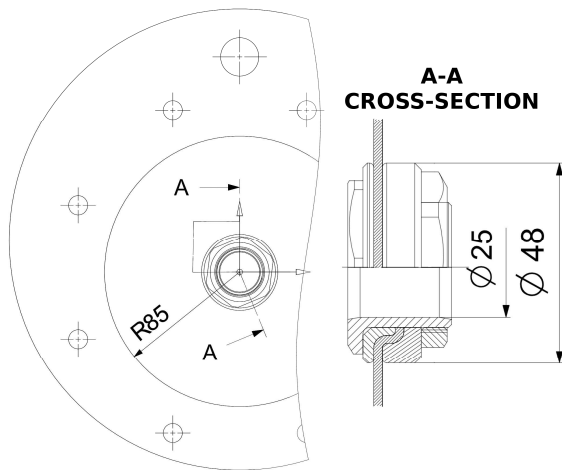


Fig. 3. Design of experimental set-up
Rys. 3. Konstrukcja elementu badawczego

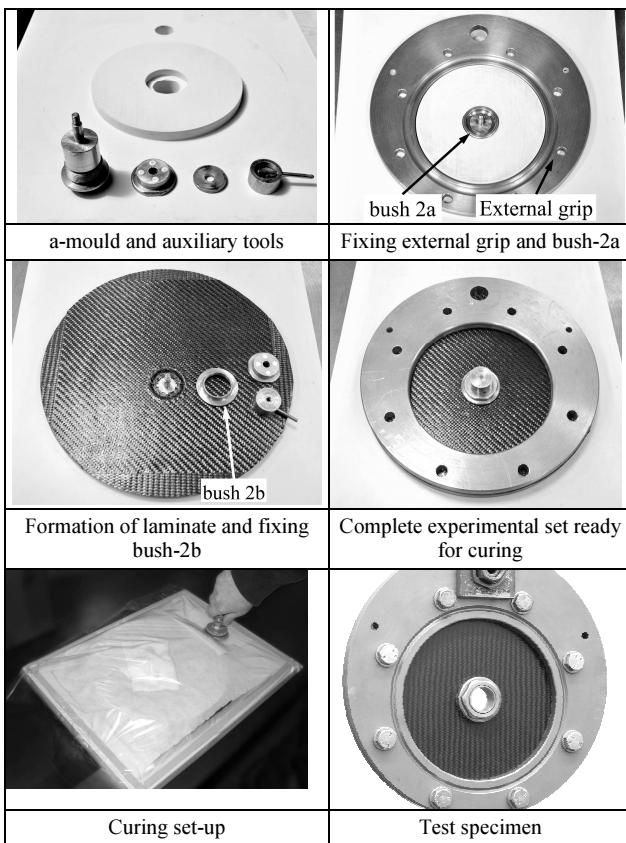


Fig. 4. Manufacturing process. Main steps
Rys. 4. Główne etapy procesu wytwarzania

FE ANALYSIS

To facilitate the subsequent experimental verification of the numerical results, the FE model was designed to represent the complete experimental setup (Fig. 5). Due to the symmetry of the set-up, just half of it was modelled. The FE analysis was carried out with ANSYS software. The mesh of the composite flange was designed in such a way that each composite layer was represented by two layers of 20-node SOLID186 brick elements (Fig 4). For proper representation of the

small radius corners of the flange, further mesh refining was done. The mesh of the outside region of the laminate consisted of 8-node SOLSH190 solid-shell elements. Interactions between all the parts of the joint were modelled with CONTA174 and TORGET170 elements allowing for taking into consideration contact forces including friction. Boundary conditions were applied according to the static test constraints including bolt pretension.

The assumed mechanical properties of the materials are listed in Table 1.

TABLE 1. Mechanical properties of MTM46/CF0300 lamina
TABELA 1. Właściwości mechaniczne powłok MTM46/CF0300

Elastic properties		
Young's moduli 1 and 2 [GPa]	$E_{11} = E_{22}$	54.5
Young's modulus 3 [GPa]	E_{33}	7.5
Poisson's ratio 1-2	ν_{12}	0.042
Poisson's ratios 1-3 and 2-3	$\nu_{13} = \nu_{23}$	0.3
Shear modulus 1-2 [MPa]	G_{12}	4430
Shear moduli 1-3 and 2-3 [MPa]	$G_{13} = G_{23}$	2500
Ultimate stress limits		
Tensile strengths 1 and 2 [MPa]	$S_{1t} = S_{2t}$	763
Tensile strength 3 [MPa]	S_{3t}	46
Compressive strengths 1 and 2 [MPa]	$S_{1c} = S_{2c}$	670
Compressive strength 3 [MPa]	S_{3c}	150
Shear strength 1-2 [MPa]	S_{12}	105
Shear strengths 1-3 and 2-3 [MPa]	$S_{13} = S_{23}$	64

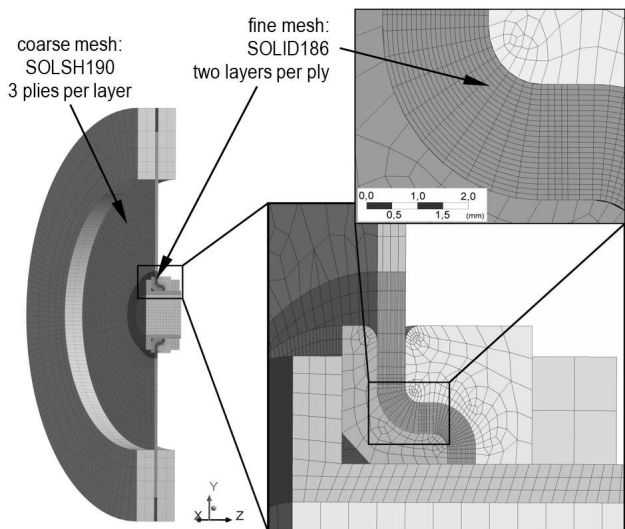


Fig. 5. Details of FE model
Rys. 5. Szczegóły modelu do analizy MES

EXPERIMENTAL WORK

The experimental investigation consisted of three parts: determining the joint load capacity, determining the strain field over the laminate plate and damage inspection. To investigate the joint load capacity two static tests were carried out. The first one ended with

complete failure of the joint marked with a total loss of its load capacity, while the second one was interrupted after the first appreciable drop in force to gain additional information on the sequence of failure events taking place in the course of loading. The corresponding load-displacement plots are shown in Figure 12. The tests were run at room temperature and at a constant cross head speed of 1.2 mm/min with the help of an Instron 8516 machine equipped with a 100 kN load cell. The experimental set-up is shown in Figure 6.

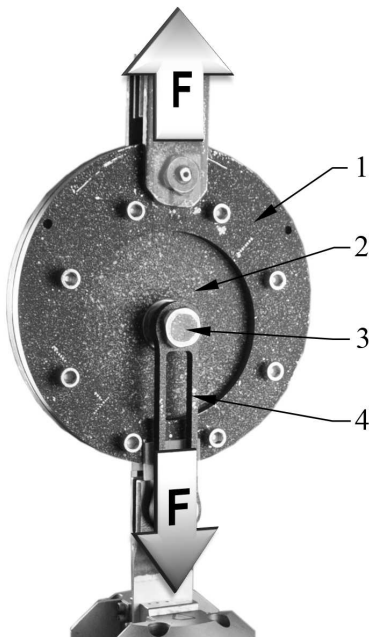


Fig. 6. Experimental set-up: 1 - metal grip, 2 - laminate plate, 3 - bolt, 4 - loading bands

Rys. 6. Zestaw badawczy: 1 - uchwyt metalowy, 2 - płyta laminatowa, 3 - sworzeń, 4 - cięgna

The strain fields over the laminate plate were determined with the help of the 3D Digital Image Correlation (DIC) method, using VIC 3D software. After the static tests, an inspection of the damage done to the laminate plates was carried out with the help of Computed Tomography (CT). For this purpose, a GE Phoenix v|tome|x s240 system was used. Only the parts of the laminate plate encompassing the flanges were investigated in order to obtain high resolution images. Two 60 mm diameter samples were prepared. The first one was cut out from the plate loaded up to complete loss of load capacity and the second one from the plate loaded up to the first appreciable drop in force.

RESULTS

The results of the FE analysis are shown in Figures 7, 8, 10, and 12. The contour plot shown in Figure 7 presents the distribution of the Inverse Reserve Factor (IRF) values for the part of the laminate encompassing the flange. The IRF was calculated based on the combined 3D maximum stress and Puck-for-woven-

materials criterion [6]. The top and bottom views of the flange are shown. The IRF values higher than one indicate laminate failure. The computed distribution of normal strain ϵ_{11} over the laminate plate in the fibre direction of the external reinforcement layer is shown in Figure 8. Due to the symmetry of the analysed structure, the distribution of ϵ_{22} was symmetrically relative to ϵ_{11} and is not shown for the purpose of picture clarity. The corresponding results of the DIC analysis are shown in Figure 9. Distribution of the normal strain in the loading direction is shown in Figure 10 and the corresponding result of the DIC analysis is shown in Figure 11. Comparison of both the computed and DIC results showed good qualitative and quantitative agreements.

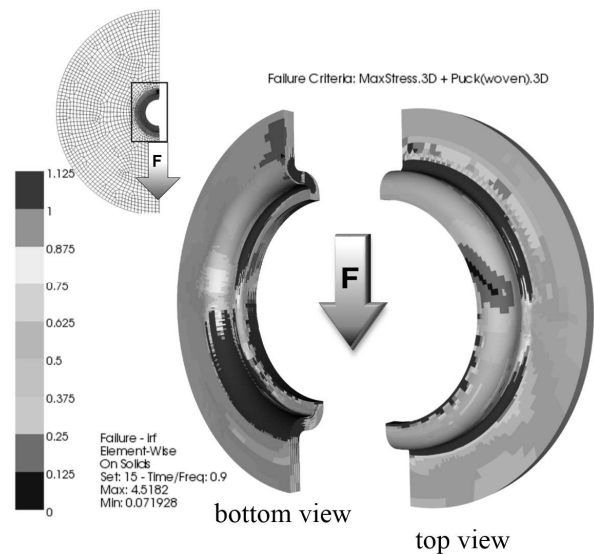


Fig. 7. Computational results for flange. Contour plot of IRF for $F = 64$ kN obtained with the help of combined 3D maximum stress and Puck-for-woven-materials failure criterion

Rys. 7. Wyniki obliczeniowe. Mapa konturowa rozkładu odwrotności współczynnika wytrzymałości przy obciążeniu $F = 64$ kN dla kombinacji kryterium maksymalnych naprężeń i Pucka dla tkanin

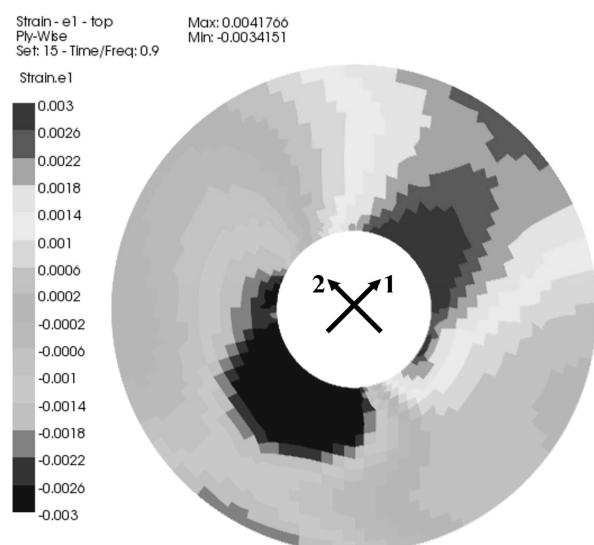


Fig. 8. Computed distribution of strains in $\theta = 45^\circ$ direction. $F \approx 62$ kN

Rys. 8. Obliczeniowe pole odkształceń w kierunku $\theta = 45^\circ$. $F \approx 62$ kN

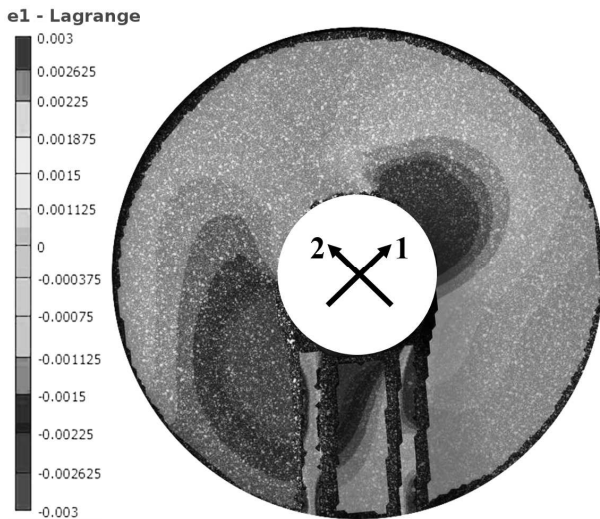


Fig. 9. Experimental (DIC) distribution of strains in $\theta = 45^\circ$ direction. $F \approx 62$ kN

Rys. 9. Doświadczalnie (DIC) wyznaczone pole odkształceń w kierunku $\theta = 45^\circ$. $F \approx 62$ kN

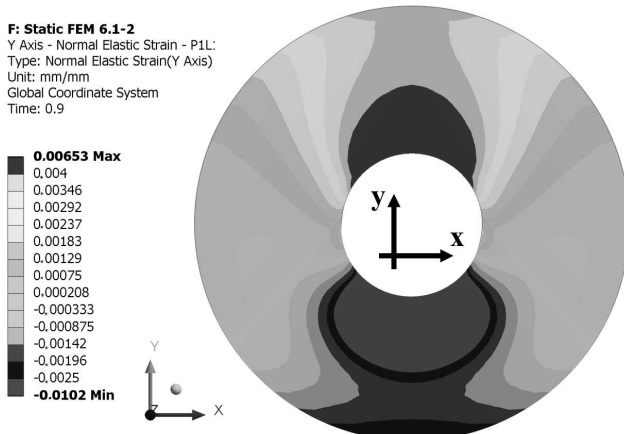


Fig. 10. Computed distribution of strains in $\theta = 0^\circ$ direction. $F \approx 62$ kN

Rys. 10. Obliczeniowe pole odkształceń w kierunku $\theta = 0^\circ$. $F \approx 62$ kN

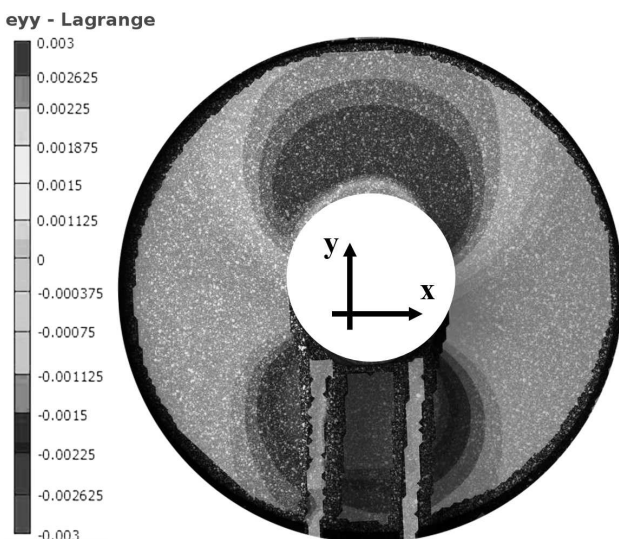


Fig. 11. Experimental (DIC) distribution of strains in $\theta = 0^\circ$ direction (loading direction). $F \approx 62$ kN

Rys. 11. Doświadczalnie (DIC) wyznaczone pole odkształceń w kierunku $\theta = 0^\circ$ (kierunek obciążenia). $F \approx 62$ kN

The calculated and experimental load-bolt displacement relationships are shown in Figure 12. The linear parts of all the plots overlaid. The FE calculations were stopped at $F = 64$ kN. The corresponding distribution of the IRF over the flange is shown in Figure 7. It can be noticed that it reached the maximum in the lower corner of the flange, suggesting that the first failure of the laminate would occur in this location. The CT results are shown in Figure 13.

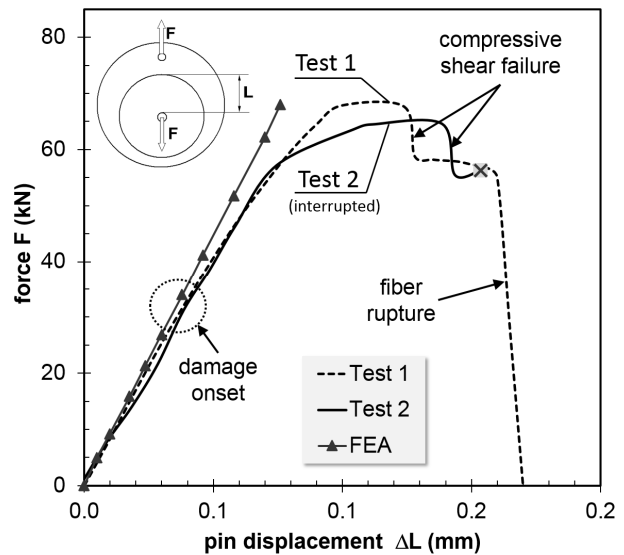


Fig. 12. Computed (FEA) and experimental load-displacement curves for static tests 1 and 2

Rys. 12. Obliczeniowy (FEA) i doświadczalny wykresy siła - przemieszczenie dla próby statycznej 1 i 2

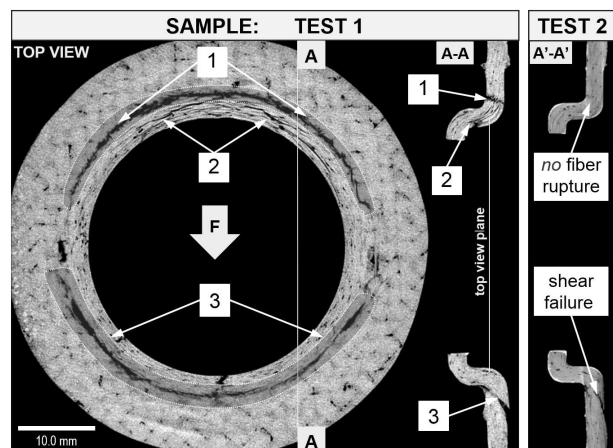


Fig. 13. CT images; Left image and cross-section A-A correspond to curve 1 in Fig. 7. Three main failure modes can be distinguished: 1 - fibre rupture, 2 - matrix cracking and matrix crack-induced delaminations, 3 - compressive shear failure. Right image (cross-section A'-A') corresponds to curve 2 in Fig. 7 and only compressive shear failure can be noticed

Rys. 13. Obrazy otrzymane za pomocą tomografii komputerowej. Obraz po prawej i przekrój A-A odpowiadają krzywej 1 obciążenie-przemieszczenie na rys. 7. Mogą być wyróżnione trzy główne postacie zniszczenia: 1 - zerwanie włókien, 2 - pęknięcia spoiwa i inicjowane tymi pęknięciami delaminacje, 3 - ścinanie laminatu na skutek działania obciążeń ściskających. Obraz po lewej (przekrój A'-A') odpowiada krzywej 2 - obciążenie-przemieszczenie na rys. 7. W tym przypadku widoczne jest jedynie uszkodzenie powstałe poprzez ścinanie w wyniku ściskania

Three main failure modes were distinguished: fibre rupture (1), matrix cracking and matrix-cracking induced delaminations (2), compressive shear (3). The association of the CT results with the load-displacement plots denoted with numbers 1 and 2 allowed the authors to conclude that the first appreciable drop in force (curve 2) could be attributed to the compressive shear failure denoted with number 3 in Figure 13b and that this failure was followed by the failures denoted with numbers 1 and 2 in Figure 13a.

CONCLUSIONS

An unconventional non-adhesive metal-composite joint was investigated with the help of FE, DIC and CT methods. Good correlation between the numerical and experimental results was obtained. Strain and stress fields in the laminate plate were determined and the way the load was transferred from the metal parts to the laminate was identified. It was proved that unlike in the case of conventional bolt joints, the laminate directly in front and behind the joint was involved in the load transfer. Furthermore, the main laminate failure modes were identified. In addition, by association of the load-displacement diagrams with the CT results, it was possible to identify the general sequence of damage events leading to total loss of the joint load capacity.

Acknowledgement

The research was funded by NCRD (National Centre for Research and Development), Poland, contract no. PBS1/B6/1/2012.

REFERENCES

- [1] Fink A., Kolesnikov B., European, hybrid titanium composite material improving composite structure coupling, *ESA SP* 2005, 581, 843-848.
- [2] Fink A., Camanho P.P., Andrés J.M., Pfeiffer E., Obst A., Hybrid CFRP/titanium bolted joints: Performance assessment and application to a spacecraft payload adaptor, *Composites Science and Technology* 2010, 70, 305-317.
- [3] Szymczyk E., Jachimowicz, J. Puchala K., Analysis of load transfer into composite structure, *Applied Computer Science* 2014, 10, 3, 86-94.
- [4] Pantelakis S., Tserpes K.I., Adhesive bonding of composite aircraft structures: Challenges and recent developments, *Sci. China-Phys Mech. Astron.* 2014, 57, 2-11.
- [5] Rodzewicz M., Input nodes of concentrated forces problem in composite structures (in Polish). *Przegląd Mechaniczny* 2004, 9, 28-32.
- [6] ANSYS® Academic Research, Release 17, Help System, ANSYS Composite PrepPost User's Guide, ANSYS, Inc.